Author Manuscript

Title: Two-Dimensional-Polycyclic Photovoltaic Molecule with Low Trap Density for High-Performance Photocatalytic Hydrogen Evolution

Authors: Zhenzhen Zhang; Wenqin Si; Baohua Wu; Wei Wang; Yawen Li; Wei Ma; Yuze Lin

To be cited as: 10.1002/anie.202114234

Link to VoR: https://doi.org/10.1002/anie.202114234

Two-Dimensional-Polycyclic Photovoltaic Molecule with Low Trap Density for High-Performance Photocatalytic Hydrogen Evolution

Zhenzhen Zhang[a,c]†, Wenqin Si[a,c]†, Baohua Wu[b], Wei Wang[a], Yawen Li[a,c], Wei Ma[b], and Yuze Lin[a,c]*

[a] Z. Zhang, W. Si, W. Wang, Y. Li, Prof. Y. Lin

Beijing National Laboratory for Molecular Sciences, CAS Key Laboratory of Organic Solids, Institute of Chemistry, Chinese Academy of Sciences, Beijing 100190, China.

Email: linyz@iccas.ac.cn

[b] B. Wu, Prof. W. Ma

State Key Laboratory for Mechanical Behavior of Materials, Xi'an Jiaotong University, Xi'an 710049, Shaanxi, China.

[c] Z. Zhang, W. Si, Y. Li, Prof. Y. Lin

University of Chinese Academy of Sciences, Beijing 100049, China.

ABSTRACT

Typical organic semiconductors show a high trap density of states (10^{16}-10^{18} cm^{-3}), providing a large number of centers for charge-carrier recombination, thus hindering the development of photocatalytic hydrogen evolution. Here, we introduce a strategy of designing and synthesizing two-dimensional-polycyclic photovoltaic material, named as TPP, to reduce the trap density as low as 2.3 $\times 10^{15}$ cm^{-3}, which is 1-3 orders of magnitudes lower than those of typical organic photovoltaic semiconductors. Moreover, TPP exhibited broad and strong absorption, ordered molecular packing with large crystalline coherence length and enhanced electron mobility. Then, the bulk heterojunction nanoparticles (BHJ-NPs) based on the blend of polymer donor (PM6) and TPP, exhibited an average hydrogen evolution rate (HER) of 72.75 mmol h^{-1} g^{-1}, which is higher than that of the control NPs based on typical PM6:Y6 (62.67 mmol h^{-1} g^{-1}) tested under 330-1100 nm illumination with light intensity of 198 mW cm^{-2}.

INTRODUCTION

Converting and storing solar energy as chemical energy, is one of the greatest available strategies to utilize the renewable and clean energy to replace fossil fuel. Solar hydrogen (H_2), as one critical green energy carriers, has high gravimetric energy density and does not generate contamination upon utilization.[1] In addition to electrolytic water, photocatalysis has been another promising option for hydrogen evolution directly from water, since water splitting using titanium oxides (TiO_2) was reported half one century ago.[2] Relative to traditional wide-bandgap inorganic or carbon nitride (CN_xH_y) photocatalysts, organic photocatalysts with facile tunable band gaps have been attracting attention as alternative materials for water splitting under illumination at visible even near-infrared (Vis-NIR) light.[3] However, organic photocatalysts, such as single semiconductor nanoparticles (NPs), and covalent organic frameworks (COFs), suffered low efficiency of charge generation owing to their short exciton diffusion length (typically 5-10 nm) [4] and high exciton binding energy (typically >300 meV), [5] limiting the efficiency enhancement of hydrogen evolution.

Polymer/organic semiconductor bulk heterojunction NPs (BHJ-NPs), in which an internal donor/acceptor heterojunction within the same NP was formed by blending photovoltaic polymer/molecule donors and acceptors, have been demonstrated to greatly enhance the efficiency of photocatalytic hydrogen evolution.[6] However, to date, very few studies focused on BHJ-NPs for hydrogen evolution, and only few photovoltaic acceptors in organic solar cells (OSCs), including IDT[6a] and IDTT[6c] based molecules, and fullerene derivatives[6b], have been introduced to fabricate BHJ-NPs. McCulloch and coworkers have first shown that PTBT-Th/EH-IDTBR BHJ-NPs could result in higher hydrogen evolution rate (HER) than those of their corresponding single-component NPs.[6a] Cooper and coworkers also obtained high HER using PCDTBT/PC_{60}BM heterojunction

NPs.[6b] Tian and coworkers introduced ternary BHJ-NPs consisting of two polymer donors and one acceptor, showing a HER of 60.8 mmol h^{-1} g^{-1}.[6c] The limited study leaves a large room for exploring how to improve the efficiency of hydrogen evolution by developing organic photovoltaic semiconductors. To our knowledge, there is still no report on designing and synthesizing new photovoltaic materials for high performance BHJ-NP photocatalytic hydrogen evolution.

Here, we designed and synthesized a two-dimensional (2D)-polycyclic photovoltaic molecule, named as TPP (chemical structure seen in **Scheme** 1), which exhibited very strong absorption at Vis-NIR range, ordered molecular packing, enhanced electron mobility and low trap density. The trap density low to around 10^{15} cm^{-3} of TPP, is 1-3 order of magnitudes lower than those (10^{16} to 10^{18} cm^{-3}) of typical organic photovoltaic semiconductors[7], and even lower than those of high-performance inorganic counterparts, like 10^{16} cm^{-3} for TiO_2.[8] The BHJ-NPs based on the blend of PM6 and TPP, with sodium 2-(3-thienyl) ethyloxybutylsulfonate (TEBS) as surfactant, exhibited an average HER of 72.75 mmol h^{-1} g^{-1} under Vis-NIR (330 to 1100 nm, 198 mW cm^{-2}) illumination for 10 h, which is higher than that of the control NPs based typical PM6:Y6 (62.67 mmol h^{-1} g^{-1}). Moreover, the average HER of PM6: TPP is over 2-3 orders higher than those values of inorganic/hybrid photocatalyst, like TiO_2 (0.321 mmol h^{-1} g^{-1})[6a] and $CH_3NH_3PbI_3$ (0.057 mmol h^{-1} g^{-1})[9].

Results and Discussion

Synthesis and Characterization of TPP

Typical linear conjugated materials exhibit low mobility due to high structural disorder and high concentrations of defect sites.[10] However, the π-electrons of 2D conjugated materials can further delocalize along the overlapped π-electron wave functions in the normal direction in addition to the main chain direction, extending the area of conjugation, decreasing structural disorder and trap density,

thus, facilitating charge carrier transport (Scheme 1).[11] The density functional theory (DFT) was employed to evaluate the geometry conformation of TPP, one 2D polycyclic photovoltaic molecule we designed here for BHJ-NP photocatalytic hydrogen evolution. To simplify the calculation, methyl groups were used to replace all alkyl side chains, which has a negligible influence on the final optimized geometry and electronic structures of molecular fused-ring skeleton. The TPP mainly consists of two planes, with a dihedral angle of *ca.* 20° (Figure S1). Moreover, the simulated highest occupied molecular orbital (HOMO) is distributed along the fused core, while the lowest unoccupied molecular orbital (LUMO) is delocalized over the entire molecule (Figure S1). The highly delocalized of π-electron of TPP is expected to behave good electron transporting.[12]

The detailed synthetic route for TPP is shown in Scheme S1 and all of the new compounds were fully characterized by spectroscopic methods (Seen in Supporting Information (SI)). Phenazines derivatives were generally obtained by a condensation reaction between diketones and diamines, and diamines can be synthesized by reduction reaction (Figure S2).[3c, 13] However, the diamine compound (Compound 3) for synthesizing TPP is easier to be obtained than diketone, and then, NH_3 is removed under acidic conditions and oxidized in air to obtain thieno[2',3':4,5]thieno[3,2-*b*]pyrrole-fused phenazines (Compound 4, Figure S2). This route is a very effective method for the synthesis of phenazines derivatives where diamines are easily available. Except for the synthesis of Compound 4, the other synthesis steps for TPP are commonly used in the synthesis of non-fullerene acceptors, such as formylated compound 5 was afforded via Vilsmeier-Haack reaction and the target molecular TPP was obtained by Knoevenagel condensation reaction.

The photocatalytic activity is highly dependent on the light-harvesting ability of the photocatalyst, especially in the Vis-NIR range where solar energy is most concentrated.[14] TPP in chloroform

solution (10^{-6} M) exhibited a high maximum extinction coefficient of 3.42×10^5 $M^{-1}cm^{-1}$ at 731 nm, which is twice that of the control Y6 (1.71×10^5 $M^{-1}cm^{-1}$).[15] Relative to its solution, the TPP film exhibited red-shifted absorption with absorption edges of 859 nm, which correspond to the optical bandgap of 1.44 eV (Figure 1a). The red-shift in TPP thin film can be attributed to strong π-π stacking interaction[16], which is supported by the analysis of crystalline properties as below. The high extinction coefficient and broad absorption range of TPP are conducive to the generation of a large number of excitons under illumination.

Crystallinity is of great significance in exciton separation and charge-carrier transport during photocatalytic activity,[17] which are the dominant factors after the generation of excitons. The molecular ordering and crystalline properties of neat TPP was investigated by grazing incidence wide-angle X-way scattering (GIWAXS, Figure 1b, 1c). TPP film exhibits out-of-plane (OOP) π-π diffraction peaks at q = 1.65 $Å^{-1}$ (d ~ 3.81 Å) with the crystalline coherence length (CCL) of 20.9 Å (calculated via Scherrer equation[18]). Another OOP peak at 0.40 $Å^{-1}$ (d ~ 15.82 Å, CCL = 106.3 Å) indicates the presence of long-distance π-π stacking in TPP film, suggesting multiple molecules stack regularly in the OOP direction.[19] Furthermore, TPP film displays regular molecular ordering in the in-plane (IP) direction, as evidenced by the presence of lamellar peak (q = 0.28 $Å^{-1}$, d ~ 22.43 Å, CCL = 191.6 Å). It is worth noting that there are two other diffraction peaks in the IP direction at q = 0.47 $Å^{-1}$ (d ~ 13.37 Å) and q = 0.56 $Å^{-1}$ (d ~ 11.22 Å), which is mostly likely to originate from the backbone stacking.[19] However, the d-spacing and CCL of Y6 are 3.63 Å, CCL = 18.2 Å in the OOP direction. In the IP direction, the d-spacing of two diffraction peaks are 23.0 Å and 15.7 Å, and CCL of two diffraction peaks are 43.2 Å and 37.7 Å, respectively.[15] Relative to Y6, enhanced CCL of TPP implied that TPP possessed stronger stacking propensity and crystallization tendency, which meant less grain

boundaries, and benefited to reduce trap density and then facilitate intermolecular charge transport. In addition, the crystallinity of TPP in powder state was investigated by X-ray diffraction (XRD, Figure S3). The XRD patterns recorded for the TPP powder exhibited diffraction peaks at 2θ = 3.99° (d = 22.16 Å), 5.39° (d = 16.40 Å), 6.62° (d = 13.36 Å), 7.72° (d = 11.46 Å) and 23.23° (d = 3.83 Å), which were very close to those diffraction peaks observed in the thin film (d = 22.43 Å, 15.82 Å, 13.37 Å, 11.22 Å and 3.81 Å). The agreement between GIWAXS of thin film and XRD of powder indicated that the crystalline nature of TPP was preserved in powder state.

The weak intermolecular interactions in organic semiconductors, especially at grain boundaries, make them susceptible to defect formation.[20] The defects in the photocatalyst are known to act as electron-hole nonradiative recombination centers, which are unfavorable for improving the photocatalytic efficiency.[21] The thermal admittance spectroscopy (TAS) method is an effective method to characterize trap density of varied energy depths in thin film and solar cell devices.[22] As shown in Figure 1d, at energy depth of 0.15-0.2 eV, the trap density of states (tDOS) of TPP is low to 2.3×10^{15} cm^{-3}, which is obviously lower than that of the control Y6 (1.1×10^{16} cm^{-3})[23], and 1-3 order of magnitudes lower than those (10^{16} to 10^{18} cm^{-3}) of typical organic photovoltaic semiconductors.[7] Compared with Y6 (4.73%), higher photoluminescence quantum yield (PLQY) of 6.69% of TPP thin film supported the less nonradiative recombination centers.[24] Nonradiative recombination centers are potential sites for charge carrier trapping. Then we estimated charge carrier mobility of organic field-effect transistors (OFETs) based TPP and Y6. TPP-based OFETs showed a higher electron mobility (μ_e) of 5.4×10^{-2} $cm^2\ V^{-1}\ s^{-1}$ (Figure 1e) than that of the Y6-based devices (2.7×10^{-2} $cm^2\ V^{-1}\ s^{-1}$, Figure S4), attributing to highly delocalized of π-electron and more order molecular stacking of TPP. Moreover, TPP exhibited more balanced electron/hole mobility (μ_h/μ_e=1.69, Figure

1e, 1f) than that of Y6 (μ_h/μ_e=3.67, Figure S4). The decreased trap density and increased electron mobility within TPP can be attributed to the enhanced molecular packing observed from GIWAXS and reduced electron-hole nonradiative recombination centers.

Photocatalytic Hydrogen Evolution

Apart from the strong optical absorption ability and high carrier transport property, efficient photogenerated exciton separation and suppression of charge carriers recombination are the overriding factors for high efficiency hydrogen production.[25] However, single-component organic semiconductor exhibited high exciton binding energy (typically >300 meV)[5] and short exciton diffusion length (typically 5-10 nm)[4], leading to low efficiency of exciton separation and a large number of charge carriers recombination. These disadvantages can alleviate by heterojunction structures providing space for delocalization of photogenerated electrons and holes.[26] For heterojunction photocatalyst, the HOMO and the LUMO levels of donors should be higher than the corresponding levels of acceptors for efficient dissociation of excitons.[26] Then, Ultraviolet photoelectron spectroscopy (UPS) and low-energy inverse photoemission spectroscopy (LEIPS) were used to calculate the energy levels of TPP (Figure S5). As shown in Figure 2a, the TPP exhibits a higher LUMO energy level (-3.89 eV) than that of Y6 (-4.03 eV)[27], meaning that TPP has more sufficient thermodynamic potential to reduce H^+ (-4.32 eV, calculation process seen in SI) relative to Y6.[14] Here, polymer donor material PM6[28] (Figure S6) is suitable to construct the D/A heterojunction, due to its lower HOMO energy level than the two-hole oxidation potential of ascorbic acid to dehydroascorbic acid (DHA/AA) and higher LUMO energy level than TPP and Y6 to achieve exciton dissociation.

In view of strong optical absorption, good charge transport and appropriate energy levels, TPP is expected to be promising for photocatalytic hydrogen evolution. To evaluate potential application of

TPP in photocatalytic hydrogen evolution, NPs, incorporated an internal PM6/TPP heterojunction, were prepared by the mini-emulsion process with TEBS as stabilizing surfactant.[29] TEBS has been demonstrated to optimize the morphology of D/A heterojunction from a core-shell structure to a intermixed blend.[6a] The size distributions of NPs containing varying PM6: TPP weight ratios were measured by dynamic light scattering (DLS) (Figure S7 and Figure 2b), which revealed that all NPs composed of a series of PM6: TPP weight ratios have a unimodal size distribution with average nanoparticle diameter at 80-130 nm. Then, we investigated the morphologies of PM6: TPP (3: 7, *w*/*w*) NPs by cryo-transmission electron microscopy (cryo-TEM, Figure 2c). PM6: TPP NPs are distributed in the photocatalytic system with the size of 89.2±13.5 nm (Figure S8a). It can be clearly observed that Pt was uniformly dispersed on the surface of the nanoparticles (Figure 2d) with size of 2.3±0.4 nm (Figure S8b), which is beneficial for electron transfer from the PM6: TPP NPs to H^+.[30] Then, we optimized the performance of hydrogen evolution by controlling donor/acceptor weight ratios, Pt ratio loadings, sacrificial electron donors, and compared HERs under different light sources, such as AM1.5 G simulated sunlight, 400-800 nm visible light and 330-1100 nm visible-NIR light (Figure S9-S12), and the details can be found in SI. The PM6: TPP (3: 7, w/w) based NPs achieved the optimized average HER of 72.75 mmol h^{-1} g^{-1} (with maximum value of 82.49 mmol h^{-1} g^{-1}) at 20% Pt loading for 10 h under 330 to 1100 nm illumination with light intensity of 198 mW cm^{-2} (Figure 2e). As shown in Figure S13, the HER of PM6: TPP NPs is much higher than those of the control single-component pure PM6 NPs (9.20 mmol h^{-1} g^{-1}) or TPP NPs (29.86 mmol h^{-1} g^{-1}), under the same test condition. The HER improvement is therefore attributed to enhanced charge generation in the PM6: TPP heterojunction, where PM6 acts as an electron donor, absorbing short-wavelength light, and TPP as an electron acceptor, absorbing long-wavelength light. The HER improvement of PM6: TPP

heterojunction is also supported by photoluminescence (PL) quenching measurement. Compared to pure PM6 NPs and pure TPP NPs, PM6: TPP heterojunction NPs show effective PL quenching yield resulting from efficient charge transfer (Figure S14). These results are consistent with published literatures.[6]

For comparison, we measured the catalytic performance of PM6:Y6 (3: 7, *w*/*w*) based NPs which showed average nanoparticle diameter of 67 nm (Figure S15). As shown in Figure S16, the optimized PM6: TPP (3: 7, *w*/*w*) NPs showed stronger absorption (from 300 nm to 820 nm) than that of PM6: Y6 NPs at the same concentration, which is beneficial to utilize photon in the area of largest solar photon flux.[31] The PM6: Y6 NPs show an average HER of 62.67 mmol h^{-1} g^{-1} (Figure S17a), which is lower than that of PM6: TPP NPs (72.75 mmol h^{-1} g^{-1}), under 330 to 1100 nm illumination (198 mW cm^{-2}) for 10 h. It should be noted here 330-1100 nm light was used because PM6: TPP NPs and PM6: Y6 NPs showed relatively broad absorption spectra to NIR range. Moreover, we also compared the catalytic performance of PM6: TPP NPs we synthesized and PTB7-Th: EH-IDTBR NPs (10% Pt) reported in the literature (absorption onset at 800 nm),[6a] under 330 to 800 nm illumination (198 mW cm^{-2}). As shown in Figure S17b, the HER of PM6: TPP NPs reached to 86.31 mmol h^{-1} g^{-1} for 10 h, which is higher than that of PTB7-Th: EH-IDTBR NPs (69.75 mmol h^{-1} g^{-1}). These results support PM6: TPP NPs have better photocatalytic performance for hydrogen evolution than PM6: Y6 NPs and PTB7-Th: EH-IDTBR NPs. Furthermore, the average HER of PM6: TPP is over 2-3 orders higher than those values of inorganic/hybrid photocatalyst, like TiO_2 (0.321 mmol h^{-1} g^{-1})[6a] and $CH_3NH_3PbI_3$ (0.057 mmol h^{-1} g^{-1})[9]. Additionally, the external quantum efficiency (EQE) of PM6: TPP NPs for photocatalytic hydrogen evolution was measured (Figure 2f). Specifically, PM6: TPP NPs achieved EQEs of higher than 7.9% at visible light wavelength of 500, 600 and 700 nm, and the EQE value can

reach 8.55% at NIR wavelength of 800 nm. The EQEs of the PM6: TPP NPs at wavelengths ≥ 500 nm are higher than PM6: Y6 NPs (Figure S18) and those reported for BHJ-NPs in literatures (Table S1).[6a, 6c]

Nonradiative Recombination and Trap Density

Although heterojunction strategy is beneficial to exciton dissociation and suppression of carrier recombination, photon energy loss is inevitable during internal conversion from light harvesting to exciton separation, especially caused by nonradiative recombination.[32]. In order to compare the nonradiative recombination of linear Y6 and 2D TPP when blending PM6 donor, we fabricated diode devices with a widely-used device structure of ITO/PEDOT: PSS/PM6: TPP or Y6/PDINN/Ag, and then studied their electroluminescence quantum efficiency (EQE_{EL}). It should be noted here that the device test is used to compare the intrinsic property of different donor/acceptor blend systems, which should qualitatively reflect the nature difference within different blend nanoparticles. The device based on PM6: TPP blend exhibits EQE_{EL} of 1.84×10^{-4} (Figure 3a), which is higher than that of PM6: Y6-based devices (1.43×10^{-4}). The higher EQE_{EL} indicated the PM6: TPP blend had weaker nonradiative recombination, relative to PM6:Y6 blend. Then, we studied the trap density of the PM6: TPP or Y6 blend films. Obviously, compared to control PM6: Y6-based devices, PM6: TPP-based devices exhibited lower tDOS with the lowest value of 3.3×10^{15} cm^{-3} (Figure 3b), which is in agreement with the observed tendency of trap density in neat films of TPP and Y6. Thus, the reduced non-radiative of PM6: TPP-based devices may be attributed to the low trap density of TPP. Relative to PM6: Y6 blend, the weaker nonradiative recombination of PM6: TPP blend due to lower trap density, should contribute to higher photocatalytic HER of PM6: TPP NPs.

Stability

Finally, we studied the photocatalytic long-term stability of PM6: TPP (3:7, w/w) NPs for 64 h, as shown in Figure S19a. After 40 h, the obvious decrease of photocatalytic reactivity is probably attributed to the lack of ascorbic acid. Thus, the cycle stability was further studied by adding a certain amount of ascorbic acid after every cycle (16 h for each cycle). As shown in Figure S19b, PM6: TPP NPs exhibited excellent stability after three cycles. Then, the photocatalytic activity began to decay in the fourth cycle, retaining 84% of the HER for the first cycle. The photocatalytic activity further decreased to 65% in the fifth cycle. Then we purified the photocatalytic solution of the fifth cycle with water (details are shown in SI), and compared the absorption spectra and size of NPs before and after stability test, to study the reasons for reduced photocatalytic activity of PM6: TPP NPs. As shown in Figure S19c, PM6: TPP NPs after stability test exhibited a nearly identical spectrum to that of the as-prepared NPs, indicating that there is no obvious material degradation of both PM6 and TPP. Furthermore, the PM6: TPP NPs after stability test shows a larger size than that of as-prepared NPs (Figure S19d), indicating the PM6: TPP NPs agglomerate after photoreaction, which may contribute to HER decrease.

CONCLUSION

In summary, we developed a two-dimensional-polycyclic photovoltaic material with reduced trap density due to ordered molecular packing. Compared to the control high performance photovoltaic materials (linear Y6, 1.1×10^{16} cm^{-3}), 2D TPP exhibited much lower trap density of 2.3×10^{15} cm^{-3}, which is also 1-3 orders of magnitudes lower than those of typical organic photovoltaic semiconductors (10^{16}-10^{18} cm^{-3}). Then, TPP showed strong absorption at visible to NIR range and enhanced electron mobility. These optical and electrical properties of TPP contributed to higher HER of PM6: TPP NPs under illumination than those of the control NPs based on typical PM6:Y6 or PTB7-

Th: EH-IDTBR. The HER of PM6: TPP NPs is also over 2-3 orders higher than those values of typical inorganic/hybrid photocatalyst in literature, such as TiO_2 and $CH_3NH_3PbI_3$. These results reveal that two-dimensional-polycyclic photovoltaic material is promising to reduce the trap density and boost the development of photocatalytic hydrogen evolution from organic semiconductors.

ASSOCIATED CONTENT

Supporting Information

Materials, Synthesis and Characterization; Scheme S1, and Figure S1-S19 and Table S1

Notes

The authors declare no competing financial interest.

ACKNOWLEDGMENTS

We acknowledge the financial support from the National Natural Science Foundation of China (52173189, 21704082, 21875182), Key Scientific and Technological Innovation Team Project of Shaanxi Province (2020TD-002), China Postdoctoral Science Foundation (2017M623162), 111 project 2.0 (BP2018008). X-ray data was acquired at beamlines 7.3.3 at the Advanced Light Source, which is supported by the Director, Office of Science, Office of Basic Energy Sciences, of the U.S. Department of Energy under Contract No. DE-AC02-05CH11231. The authors thank Chenhui Zhu at beamline 7.3.3 for assistance with data acquisition. We thank the PLQY measurement help of Dr. Stuart Thomson and Dr. Marco Ferreira from Edinburgh instruments. We thank Prof. Yilin Wang from Institute of Chemistry, Chinese Academy of Sciences for the DLS measurement. We thank Dr. Bo

Guan, Jiling Yue and Kaiang Liu from Institute of Chemistry, Chinese Academy of Sciences for the cryo-TEM measurement. Z. Z. and W. S. contributed equally to this work.

Keywords: • photocatalytic hydrogen evolution • two-dimensional-polycyclic material • trap density • bulk heterojunction nanoparticle • solar hydrogen

REFERENCE

[1] a) T. Hisatomi, K. Domen, *Nat. Catal.* **2019**, *2*, 387-399; b) S. Chen, T. Takata, K. Domen, *Nat. Rev. Mater.* **2017**, *2*, 17050; c) J. Zhu, L. Hu, P. Zhao, L. Y. S. Lee, K. Y. Wong, *Chem. Rev.* **2020**, *120*, 851-918.

[2] A. Fujishima, K. Honda, *Nature* **1972**, *238*, 37-38.

[3] a) J. Kosco, M. Sachs, R. Godin, M. Kirkus, L. Francas, M. Bidwell, M. Qureshi, D. Anjum, J. R. Durrant, I. McCulloch, *Adv. Energy Mater.* **2018**, *8*, 1802181; b) V. S. Vyas, V. W.-h. Lau, B. V. Lotsch, *Chem. Mater.* **2016**, *28*, 5191-5204; c) G. Zhang, Z. A. Lan, X. Wang, *Angew. Chem. Int. Ed.* **2016**, *55*, 15712-15727; *Angew. Chem.* **2016**, *128*, 15940–15956; d) L. Wang, R. Fernandez-Teran, L. Zhang, D. L. Fernandes, L. Tian, H. Chen, H. Tian, *Angew. Chem. Int. Ed.* **2016**, *55*, 12306-12310; *Angew. Chem.* **2016**, *128*, 12494–12498.

[4] a) O. V. Mikhnenko, P. W. M. Blom, T.-Q. Nguyen, *Energy Environ. Sci.* **2015**, *8*, 1867-1888; b) G. J. Hedley, A. J. Ward, A. Alekseev, C. T. Howells, E. R. Martins, L. A. Serrano, G. Cooke, A. Ruseckas, I. D. W. Samuel, *Nat. Commun.* **2013**, *4*, 2867.

[5] a) L. Zhu, Y. Yi, Z. Wei, *J. Phys. Chem. C* **2018**, *122*, 22309-22316; b) S. Kraner, R. Scholz, C. Koerner, K. Leo, *J. Phys. Chem. C* **2015**, *119*, 22820-22825.

[6] a) J. Kosco, M. Bidwell, H. Cha, T. Martin, C. T. Howells, M. Sachs, D. H. Anjum, S. Gonzalez Lopez, L. Zou, A. Wadsworth, W. Zhang, L. Zhang, J. Tellam, R. Sougrat, F. Laquai, D. M. DeLongchamp, J. R. Durrant, I. McCulloch, *Nat. Mater.* **2020**, *19*, 559-565; b) H. Yang, X. Li, R. S. Sprick, A. I. Cooper, *Chem. Commun.* **2020**, *56*, 6790-6793; c) A. Liu, L. Gedda, M. Axelsson, M. Pavliuk, K. Edwards, L. Hammarstrom, H. Tian, *J. Am. Chem. Soc.* **2021**, *143*, 2875-2885.

[7] a) J. A. Carr, S. Chaudhary, *Energy Environ. Sci.* **2013**, *6*, 3414-3438; b) M. Geiger, L. Schwarz, U. Zschieschang, D. Manske, J. Pflaum, J. Weis, H. Klauk, R. T. Weitz, *Phys. Rev. Appl.* **2018**, *10*, 044023; c) W. L. Kalb, S. Haas, C. Krellner, T. Mathis, B. Batlogg, *Phys. Rev. B* **2010**, *81*, 155315.

[8] a) S. Nakayashiki, H. Daisuke, Y. Ogomi, S. Hayase, *J. Photon. Energy* **2015**, *5*, 057410; b) H. Tao, J. Li, C. Zhang, L. Ding, W. Zhang, J. Xiao, *Mater. Chem. Phys.* **2020**, *254*, 123436.

[9] S. Park, W. J. Chang, C. W. Lee, S. Park, H.-Y. Ahn, K. T. Nam, *Nat. Energy* **2016**, *2*, 16185.

[10] D. Burmeister, M. G. Trunk, M. J. Bojdys, *Chem. Soc. Rev.* **2021**, *50*, 11559-11576.

[11] a) Y.-W. Su, Y.-C. Lin, K.-H. Wei, *J. Mater. Chem. A* **2017**, *5*, 24051-24075; b) Z. A. Li, C. C. Chueh, A. K. Y. Jen, *Prog. Polym. Sci.* **2019**, *99*, 101175.

[12] C. Yao, Y. Yang, L. Li, M. Bo, C. Peng, J. Wang, *J. Mater. Chem. A* **2019**, *7*, 18150-18157.

[13] Y. Xie, T. Fujimoto, S. Dalgleish, Y. Shuku, M. M. Matsushita, K. Awaga, *J. Mater. Chem. C* **2013**, *1*, 3467-3481.

[14] J. Kosco, F. Moruzzi, B. Willner, I. McCulloch, *Adv. Energy Mater.* **2020**, *10*, 2001935.

[15] Z. Zhang, Y. Li, G. Cai, Y. Zhang, X. Lu, Y. Lin, *J. Am. Chem. Soc.* **2020**, *142*, 18741-18745.

[16] Y. Deng, W. Yuan, Z. Jia, G. Liu, *J. Phys. Chem. B* **2014**, *118*, 14536-14545.

[17] Y. Guo, J. Li, Y. Yuan, L. Li, M. Zhang, C. Zhou, Z. Lin, *Angew. Chem. Int. Ed.* **2016**, *55*, 14693-14697; *Angew. Chem.* **2016**, *128*, 14913–14917.

[18] D.-M. Smilgies, *J. Appl. Crystallogr.* **2013**, *46*, 286-286.

[19] G. Zhang, X.-K. Chen, J. Xiao, P. C. Y. Chow, M. Ren, G. Kupgan, X. Jiao, C. C. S. Chan, X. Du, R. Xia, Z. Chen, J. Yuan, Y. Zhang, S. Zhang, Y. Liu, Y. Zou, H. Yan, K. S. Wong, V. Coropceanu, N. Li, C. J. Brabec, J.-L. Bredas, H.-L. Yip, Y. Cao, *Nat. Commun.* **2020**, *11*, 3943.

[20] H. F. Haneef, A. M. Zeidell, O. D. Jurchescu, *J. Mater. Chem. C* **2020**, *8*, 759-787.

[21] a) M. Z. Rahman, M. G. Kibria, C. B. Mullins, *Chem. Soc. Rev.* **2020**, *49*, 1887-1931; b) L. Zhang, J. Ran, S. Z. Qiao, M. Jaroniec, *Chem. Soc. Rev.* **2019**, *48*, 5184-5206.

[22] D. O. Scanlon, C. W. Dunnill, J. Buckeridge, S. A. Shevlin, A. J. Logsdail, S. M. Woodley, C. R. A. Catlow, M. J. Powell, R. G. Palgrave, I. P. Parkin, G. W. Watson, T. W. Keal, P. Sherwood, A. Walsh, A. A. Sokol, *Nat. Mater.* **2013**, *12*, 798-801.

[23] Y. Zhang, G. Cai, Y. Li, Z. Zhang, T. Li, X. Zuo, X. Lu, Y. Lin, *Adv. Mater.* **2021**, *33*, 2008134.

[24] I. G. Scheblykin, *Adv. Energy Mater.* **2020**, *10*, 2001724.

[25] C. Ye, J.-X. Li, Z.-J. Li, X.-B. Li, X.-B. Fan, L.-P. Zhang, B. Chen, C.-H. Tung, L.-Z. Wu, *ACS Catal.* **2015**, *5*, 6973-6979.

[26] J. Low, J. Yu, M. Jaroniec, S. Wageh, A. A. Al-Ghamdi, *Adv. Mater.* **2017**, *29*, 1601694.

[27] T. Li, K. Wang, G. Cai, Y. Li, H. Liu, Y. Jia, Z. Zhang, X. Lu, Y. Yang, Y. Lin, *JACS Au* **2021**, *1*, 1733-1742.

[28] S. Karuthedath, J. Gorenflot, Y. Firdaus, N. Chaturvedi, C. S. P. De Castro, G. T. Harrison, J. I. Khan, A. Markina, A. H. Balawi, T. A. D. Peña, W. Liu, R.-Z. Liang, A. Sharma, S. H. K. Paleti, W. Zhang, Y. Lin, E. Alarousu, S. Lopatin, D. H. Anjum, P. M. Beaujuge, S. De Wolf, I.

McCulloch, T. D. Anthopoulos, D. Baran, D. Andrienko, F. Laquai, *Nat. Mater.* **2021**, *20*, 378-384.

[29] L. Stegbauer, K. Schwinghammer, B. V. Lotsch, *Chem. Sci.* **2014**, *5*, 2789-2793.

[30] J. R. McKone, S. C. Marinescu, B. S. Brunschwig, J. R. Winkler, H. B. Gray, *Chem. Sci.* **2014**, *5*, 865-878.

[31] Y. Li, Z. Wang, T. Xia, H. Ju, K. Zhang, R. Long, Q. Xu, C. Wang, L. Song, J. Zhu, J. Jiang, Y. Xiong, *Adv. Mater.* **2016**, *28*, 6959-6965.

[32] M. Rahman, H. Tian, T. Edvinsson, *Angew. Chem. Int. Ed.* **2020**, *59*, 16278-16293; *Angew. Chem.* **2020**, *132*, 16418–16433.

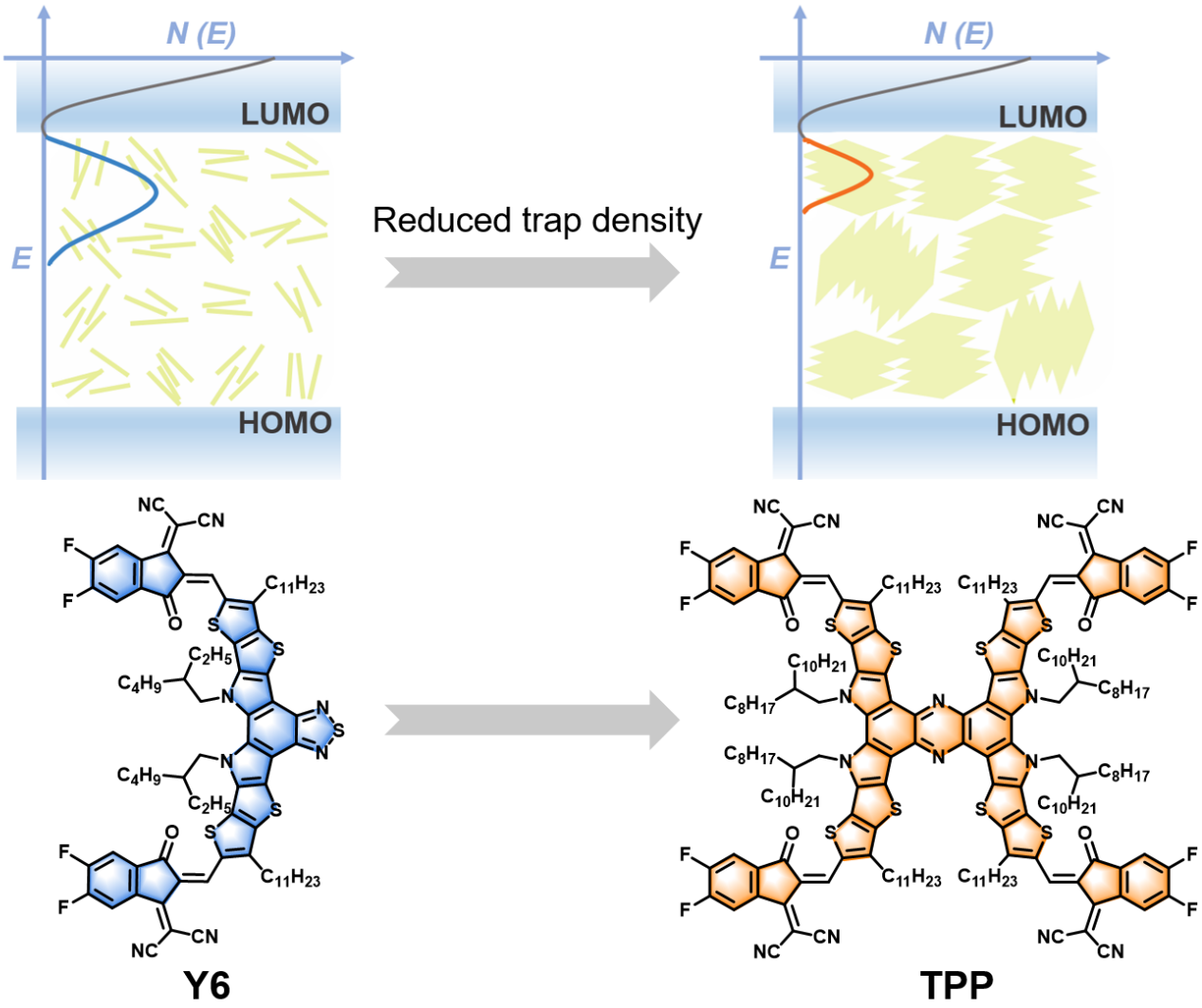

Scheme 1. The diagram of the motivation to study 2D conjugated materials. Relative to linear conjugated materials, the 2D conjugated materials exhibit lower structural disorder and trap density, which benefit higher charge carrier transport. The green line stands for linear conjugated materials, and the green rectangle stands for 2D conjugated materials. The blue and orange curves stand for trap state.

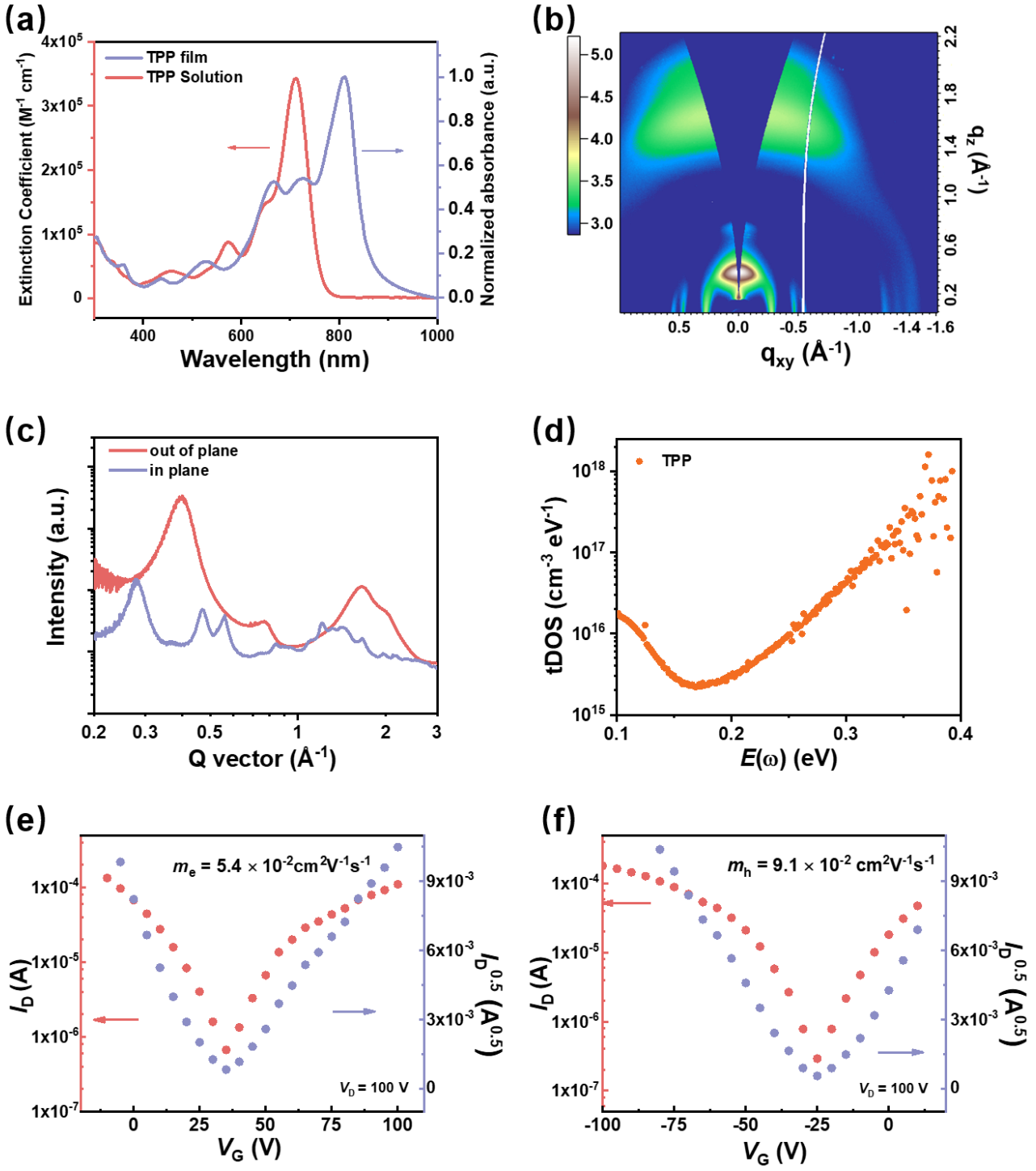

Figure 1. (a) Absorption spectra of TPP in chloroform solution and the absorption spectra of TPP film. Two-dimensional GIWAXS patterns (b) and profiles (c) of neat TPP film. (d) Trap density of states spectra of TPP based devices. Transfer characteristics of n-channel OFET (e) and p-channel OFET (f) with TPP.

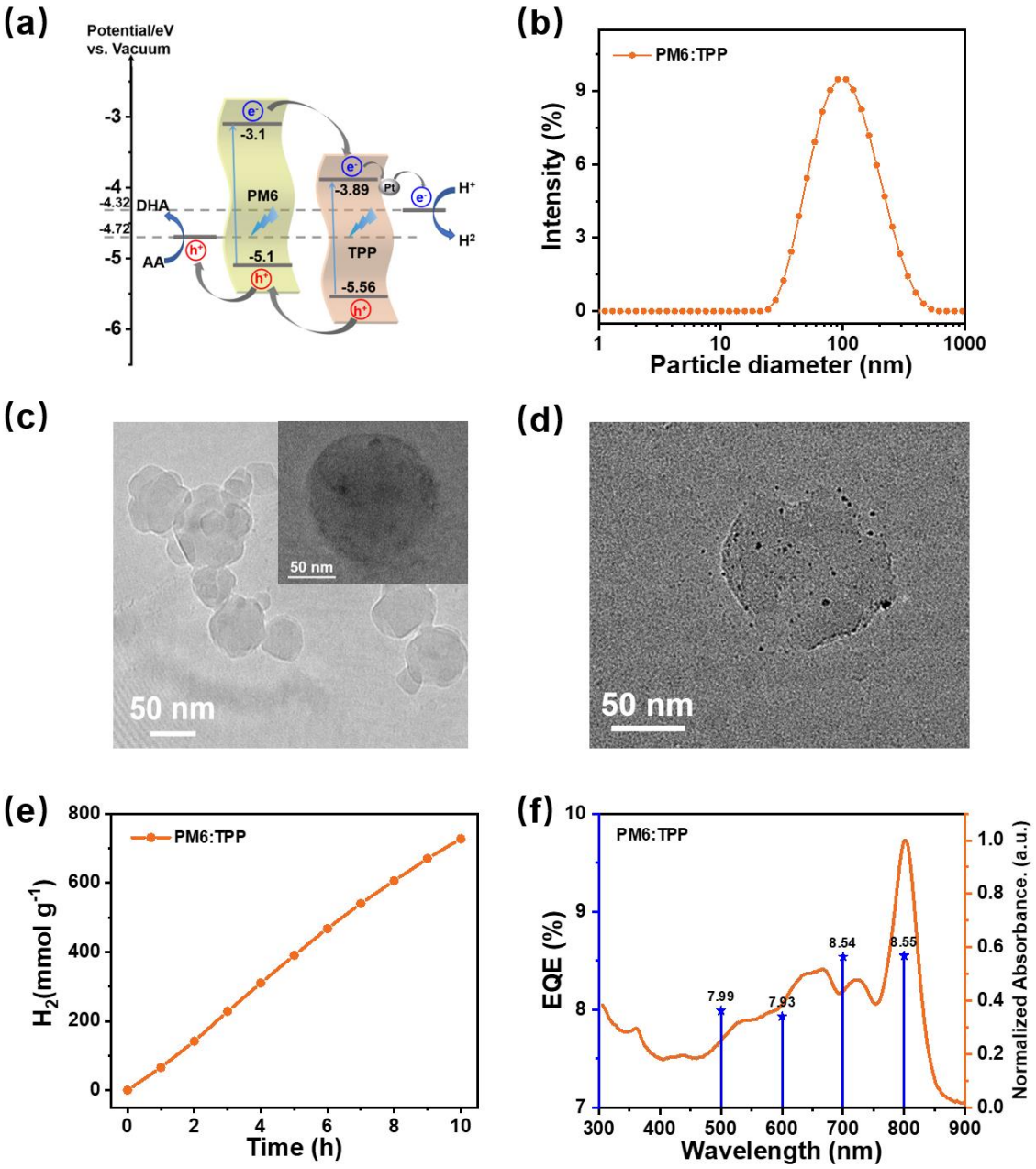

Figure 2. (a) Energy levels of PM6 and TPP compared to the proton reduction potential (H^+/H_2) and the calculated potential (DHA/AA) at pH=2 (the pH of 0.2 mol L^{-1} AA).[6a] (b) DLS size distributions by intensity of PM6: TPP NPs (3: 7, *w*/*w*). (c) Cryo-TEM of PM6: TPP NPs without Pt loading. Inset show the zoom-in single NP image. (d) Cryo-TEM of PM6: TPP NPs with 20% Pt loading. The black dots are Pt. (e) H_2 evolution versus time of PM6: TPP NPs (3: 7, *w*/*w*) under 330 to 1100 nm illumination with light intensity of 198 mW cm^{-2}. (f) EQE at 500, 600, 700 and 800 nm and absorption

spectrum of PM6: TPP NPs (3: 7, *w*/*w*) photocatalysts.

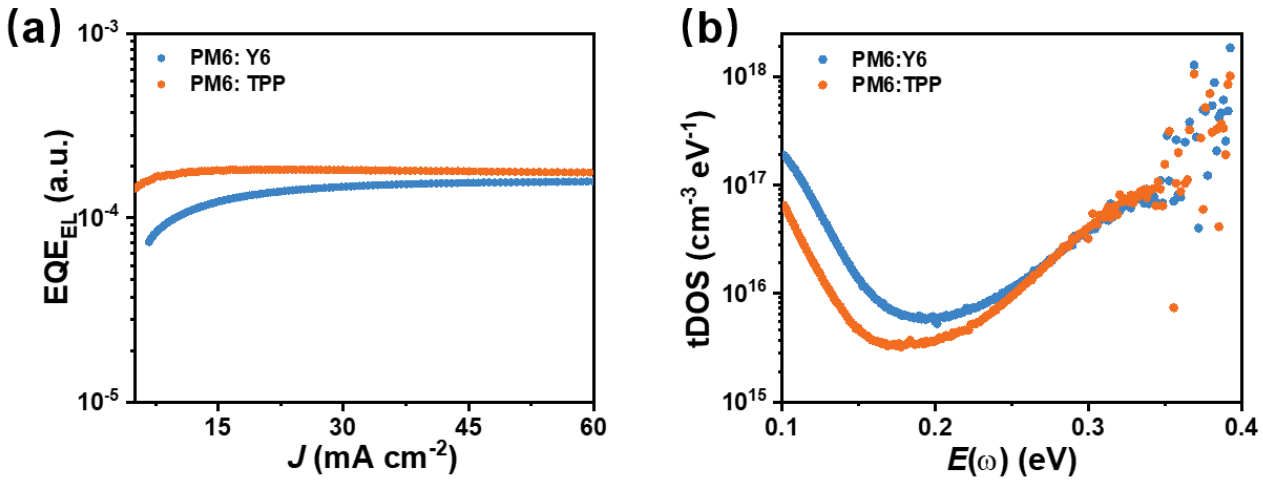

Figure 3. (a) EQE_{EL} and (b) tDOS spectra of PM6: TPP- and PM6: Y6-based devices.

TOC

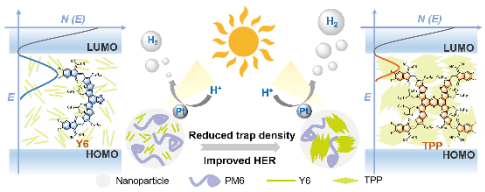

Compared to typical linear conjugated materials (Y6), two-dimensional-polycyclic material (TPP) designed and synthesized here exhibit much lower trap density. The bulk heterojunction nanoparticles based on the blend of polymer donor and TPP, exhibited an enhanced average hydrogen evolution rate of 72.75 mmol h^{-1} g^{-1} under 330 to 1100 nm illumination, which is 2-3 orders higher than those values of inorganic/hybrid photocatalysts.